

ELECTRON BEAM DYNAMICS OPTIMIZATION USING A UNIFIED DIFFERENTIAL EVOLUTION ALGORITHM*

J. Qiang[†] and C. E. Mitchell, LBNL, Berkeley, CA 94720, USA

Abstract

Accelerator beam dynamics design depends heavily on the use of control parameter optimization to achieve the best performance. In this paper, we report on electron beam dynamics optimization of a model photoinjector using a new unified differential evolution algorithm. We present the new unified differential evolution algorithm and benchmark its performance using several test examples. We also discuss the application of the algorithm in the multi-objective optimization of the photoinjector.

INTRODUCTION

The photoinjector is a key component in the accelerator beam delivery system of next generation light sources, generating a high brightness electron beam into the accelerator. The goal of photoinjector beam dynamics design is to achieve a high peak current while maintaining low transverse emittances at the same time. This requires optimizing a number of physical control parameters such as accelerating RF cavity amplitudes and phases, focusing solenoid strengths and locations, and the initial distribution of the electron beam. In previous studies, multi-objective optimization based on genetic algorithms has been used in the photoinjector beam dynamics optimization [1–3]. In this paper, we apply a new unified differential evolution algorithm for multi-objective beam dynamics optimization.

The differential evolution algorithm is a relatively new method in evolutionary algorithms [4]. It is a simple but powerful population-based, stochastic, direct-search algorithm with self-adaptive step size to generate next-generation offspring for global optimization. In a number of comparison studies, it has been shown to be efficient in comparison to simulated annealing method, controlled random search, evolutionary programming, and genetic algorithms [4–6]. However, the standard differential evolution algorithm includes multiple strategies during the mutation stage. This could complicate the use of the algorithm. In this paper, we have adopted a unified differential algorithm recently proposed by the authors [7] in a newly developed variable population multi-objective differential evolution algorithm [8] in a photoinjector beam dynamics optimization.

STANDARD DIFFERENTIAL EVOLUTION

In the standard differential evolution algorithm, a population with size NP in control parameter space is randomly generated at the beginning. This population defines the first

generation of the control parameters. After this initialization, the differential evolution algorithm consists of three stages to produce a new generation: mutation, crossover, and selection. During the mutation stage, for each parameter vector $\vec{x}_{i,G}, i = 0, 1, 2, \dots, NP - 1$ in a population of size NP at generation G , a perturbed vector \vec{v}_i is generated using one of the following mutation strategies [4, 9]:

$$\text{DE/rand/1} : \vec{v}_i = \vec{x}_{r_1} + F_{xc}(\vec{x}_{r_2} - \vec{x}_{r_3}) \quad (1)$$

$$\text{DE/rand/2} : \vec{v}_i = \vec{x}_{r_1} + F_{xc}(\vec{x}_{r_2} - \vec{x}_{r_3}) + F_{xc}(\vec{x}_{r_4} - \vec{x}_{r_5}) \quad (2)$$

$$\text{DE/best/1} : \vec{v}_i = \vec{x}_b + F_{xc}(\vec{x}_{r_1} - \vec{x}_{r_2}) \quad (3)$$

$$\text{DE/best/2} : \vec{v}_i = \vec{x}_b + F_{xc}(\vec{x}_{r_1} - \vec{x}_{r_2}) + F_{xc}(\vec{x}_{r_3} - \vec{x}_{r_4}) \quad (4)$$

$$\text{DE/current-to-best/1} : \vec{v}_i = \vec{x}_i + F_{cr}(\vec{x}_b - \vec{x}_i) + F_{xc}(\vec{x}_{r_1} - \vec{x}_{r_2}) \quad (5)$$

$$\text{DE/current-to-best/2} : \vec{v}_i = \vec{x}_i + F_{cr}(\vec{x}_b - \vec{x}_i) + F_{xc}(\vec{x}_{r_1} - \vec{x}_{r_2}) + F_{xc}(\vec{x}_{r_3} - \vec{x}_{r_4}) \quad (6)$$

$$\text{DE/current-to-rand/1} : \vec{v}_i = \vec{x}_i + F_{cr}(\vec{x}_{r_1} - \vec{x}_i) + F_{xc}(\vec{x}_{r_2} - \vec{x}_{r_3}) \quad (7)$$

$$\text{DE/current-to-rand/2} : \vec{v}_i = \vec{x}_i + F_{cr}(\vec{x}_{r_1} - \vec{x}_i) + F_{xc}(\vec{x}_{r_2} - \vec{x}_{r_3}) + F_{xc}(\vec{x}_{r_4} - \vec{x}_{r_5}) \quad (8)$$

$$\text{DE/rand-to-best/1} : \vec{v}_i = \vec{x}_{r_1} + F_{cr}(\vec{x}_b - \vec{x}_i) + F_{xc}(\vec{x}_{r_2} - \vec{x}_{r_3}) \quad (9)$$

$$\text{DE/rand-to-best/2} : \vec{v}_i = \vec{x}_{r_1} + F_{cr}(\vec{x}_b - \vec{x}_i) + F_{xc}(\vec{x}_{r_2} - \vec{x}_{r_3}) + F_{xc}(\vec{x}_{r_4} - \vec{x}_{r_5}) \quad (10)$$

where the integers r_1, r_2, r_3, r_4 and r_5 are chosen randomly from the interval $[1, NP]$ and are different from the current index i , F_{xc} is a real scaling factor that controls the amplification of the differential variation, \vec{x}_b is the best solution among the NP population members at the generation G , and F_{cr} is a weight for the combination between the original target vector and the best parent vector or the random parent vector. In order to increase the diversity of the parameter vectors, crossover between the parameter vector $\vec{x}_{i,G}$ and the perturbed vector \vec{v}_i is introduced with an externally supplied crossover probability Cr to generate a new trial vector $U_{i,G+1}, i = 0, 1, 2, \dots, NP - 1$. For a D dimensional control parameter space, the new trial parameter vector $U_{i,G+1}, i = 0, 1, 2, \dots, NP - 1$ is generated using the following rule:

$$\vec{U}_i = (u_{i1}, u_{i2}, \dots, u_{iD}) \quad (11)$$

$$u_{ij} = \begin{cases} v_{ij}, & \text{if } \text{rand}_j \leq CR \text{ or } j = \text{mbr}_i \\ x_{ij}, & \text{otherwise} \end{cases} \quad (12)$$

where rand_j is a randomly chosen real number in the interval $[0, 1]$, and the index mbr_i is a randomly chosen in-

* Work supported by the U.S. Department of Energy under Contract No. DE-AC02-05CH11231.

[†] jqiang@lbl.gov

teger in the range $[1, D]$ to ensure that the new trial vector contains at least one parameter from the perturbed vector. During the selection stage, the new trial solution $U_{i,G+1}$ is checked against the original parent $x_{i,G}$. If the new trial solution produces a better objective function value, it will be put into the next generation $(G + 1)$ population. Otherwise, the original parent is kept in the next generation population. The above procedure is repeated for all NP parents to populate a new generation. This completes one new generation. Many generations are used to attain the final global optimal solution.

THE UNIFIED DIFFERENTIAL EVOLUTION ALGORITHM

The presence of multiple mutation strategies can complicate the use of the differential evolution algorithm. A new single mutation expression that can unify most conventional mutation strategies used by the differential evolution algorithm was proposed by the authors [7]. This single unified mutation expression can be written as:

$$\vec{v}_i = \vec{x}_i + F_1(\vec{x}_b - \vec{x}_i) + F_2(\vec{x}_{r_1} - \vec{x}_i) + F_3(\vec{x}_{r_2} - \vec{x}_{r_3}) + F_4(\vec{x}_{r_4} - \vec{x}_{r_5}) \quad (13)$$

Here, the second term on the right hand of the equation (13) denotes the contribution from the best found solution in the current generation, the third term denotes the rotationally invariant contribution from the random solution, and the fourth and fifth terms are the same terms as those used in the original differential evolution algorithm to account for the contributions from the difference of parent solutions. The four parameters F_1 , F_2 , F_3 and F_4 are the weights from each contribution. This unified mutation expression represents a combination of exploitation (from the best found solution) and exploration (from the random solutions) to generate a new mutant solution.

From the above equation, one can see that for $F_1 = 0$, $F_2 = 1$, and $F_4 = 0$, this equation reduces to DE/rand/1; for $F_1 = 0$, $F_2 = 1$, and $F_3 = F_4$, it reduces to DE/rand/2; for $F_1 = 1$, $F_2 = 0$, and $F_4 = 0$, it reduces to DE/best/1; for $F_1 = 1$, $F_2 = 0$, and $F_3 = F_4$, it reduces to DE/best/2; for $F_2 = 0$ and $F_4 = 0$, it reduces to DE/current-to-best/1; for $F_2 = 0$ and $F_3 = F_4$, it reduces to DE/current-to-best/2; for $F_1 = 0$, and $F_4 = 0$, it reduces to DE/current-to-rand/1; for $F_1 = 0$, and $F_3 = F_4$, it reduces to DE/current-to-rand/2; for $F_2 = 1$, and $F_4 = 0$, it reduces to DE/rand-to-best/1; for $F_2 = 1$, and $F_3 = F_4$, it reduces to DE/rand-to-best/2. Using the single equation (13), ten mutation strategies in the standard differential evolution algorithm can be written as a single mutation expression. Meanwhile, this new expression provides an opportunity to explore more broadly the space of mutation operators. By using a different set of parameters F_1, F_2, F_3, F_4 , a new mutation strategy can be achieved. For example, from our experience, we found that using $F_1 = 0.25$, $F_2 = 0.25$, $F_3 = 0.2$, $F_4 = 0.2$, and $CR = 0.8$ in the uDE can give better performance in some test studies than the conventional mutation strategy [4, 9]

(shown in the following section). If these parameters can be adaptively adjusted during the optimization evolution, then multiple mutation strategies and their combinations can be used during different stages of optimization. Thus, the unified mutation expression has the virtue of mathematical simplicity and also provides the user with flexibility for broader exploration of different mutation strategies.

BENCHMARK EXAMPLES

One of the exploratory unified differential evolution algorithms (uDE) ($F_1 = 0.25, F_2 = 0.25, F_3 = 0.2, F_4 = 0.2, CR = 0.8$) is tested with several numerical test functions together with the conventional differential evolution algorithm. These test functions are [10, 11]:

- (1) Sphere function

$$F_{\text{sph}}(\vec{x}) = \sum_{i=1}^N x_i^2; \quad -100 \leq x_i \leq 100;$$

- (2) Schwefel's problem 1.2

$$F_{\text{sch2}}(\vec{x}) = \sum_{j=1}^N \left(\sum_{i=1}^j x_i \right)^2; \quad -100 \leq x_i \leq 100;$$

- (3) Quartic function with noise

$$F_{\text{qrt}}(\vec{x}) = \sum_{i=1}^N i x_i^4 + \text{rand}[0, 1]; \quad -1.28 \leq x_i \leq 1.28;$$

- (4) Ackley's function

$$F_{\text{ack}}(\vec{x}) = 20 + \exp(1) - 20 \exp\left(-0.2 \sqrt{\frac{1}{N} \sum_{i=1}^N x_i^2}\right) - \exp\left(\frac{1}{N} \sum_{i=1}^N \cos(2\pi x_i)\right); \quad -32 \leq x_i \leq 32;$$

The sphere function is a continuous, unimodal and separable function. The Schwefel's problem 1.2 is a non-separable unimodal function. The noisy quartic function is a unimodal function with random noise in the objective value. The Ackley's function is a multimodal non-separable problem and has many local minima and a narrow global minimum.

In Figs. 1-4, we show the evolution of the error relative to the true global minimum objective function value of these test functions for the algorithms with dimension $N = 50$. At each generation, the objective function value has been averaged over 25 random seeds. It is seen that the unified differential algorithm performs quite well in these test examples quickly converging to the true minimum.

A PHOTOINJECTOR BEAM DYNAMICS OPTIMIZATION

We applied the above exploratory unified differential evolution algorithm together with a particle-in-cell code [12]

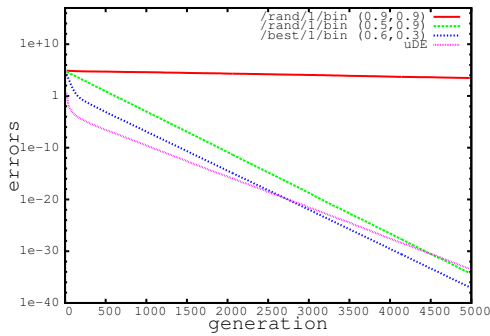


Figure 1: Evolution of the average error in the test sphere function.

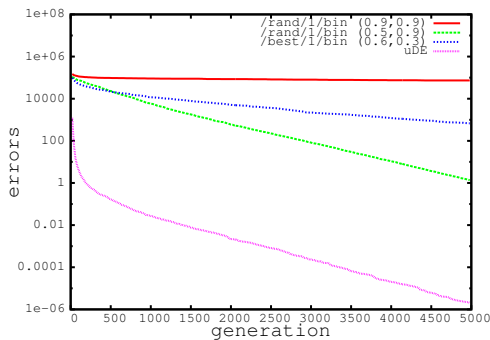


Figure 2: Evolution of the average error in the test Schwefel's problem 1.2 function.

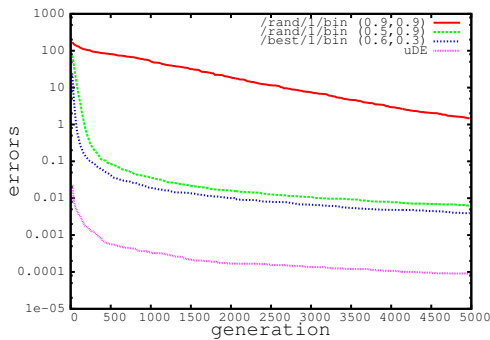


Figure 3: Evolution of the average error in the noisy quartic function.

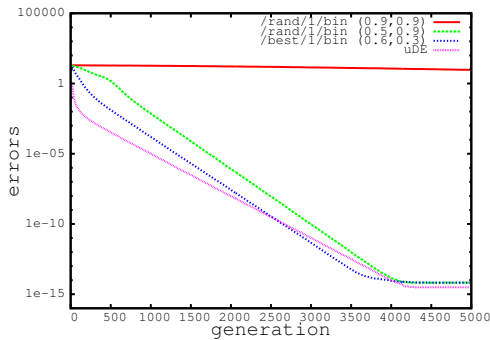


Figure 4: Evolution of the average error in the Ackley function.

in a photoinjector beam dynamics optimization. This unified differential algorithm was implemented in the recently developed multi-objective differential evolution algorithm based on the variable population and external storage for beam dynamics optimization [8]. A schematic plot of the photoinjector is shown in Fig. 5. It consists of a 187 MHz

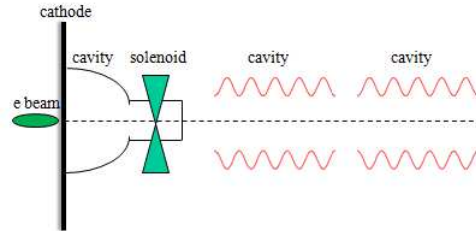


Figure 5: A schematic plot of a photoinjector for multi-objective optimization application.

RF gun [13, 14], a solenoid, and two 1.3 GHz boosting cavities. The objective functions to be optimized are the transverse rms emittances and the longitudinal rms bunch length that is directly related to the peak current of the beam. There are 9 control parameters that are used in the optimization. Those are the initial electron beam transverse size and bunch length, strength of the solenoid field, starting location of the boosting RF cavity, and amplitudes and phases of the two RF cavities. The maximum amplitude of the RF field inside the gun is set as about 38 MV/m. The charge for the electron beam is 300 pC. Some optimal solutions of the rms bunch length and the transverse emittance are shown in Fig. 6. There is a sharp change of the rms bunch length around rms emittance 1.4 mm-mrad. This sharp reduction of the rms bunch length is due to the over compression of the electron beam longitudinally. In the photoinjector design, one normally tries to keep the final transverse emittance below 1 mm-mrad. Here, we choose a working point with transverse emittance around 0.9 mm-mrad. Figure 7 shows the rms projected emittance evolution inside the injector. At the end of the second boosting RF cavity, the transverse rms emittance reaches 0.9 mm-mrad, but still decreases. The kinetic energy of the beam at the exit of the second cavity is about 13 MeV with a final peak current of 20 A.

SUMMARY AND DISCUSSION

In this paper, we used a new unified differential evolution algorithm in the multi-objective photoinjector beam dynamics optimization. The unified differential evolution algorithm has the virtue of mathematical simplicity and the capability to explore a broader mutation strategy space. Using a new exploratory mutation strategy, we have done beam dynamics optimization for a photoinjector consisting of a low RF frequency gun, a solenoid and two boosting cavity. Our preliminary optimization results suggest that below 1 um transverse emittance is achievable out of this injector. More detailed study is needed to understand the space-charge

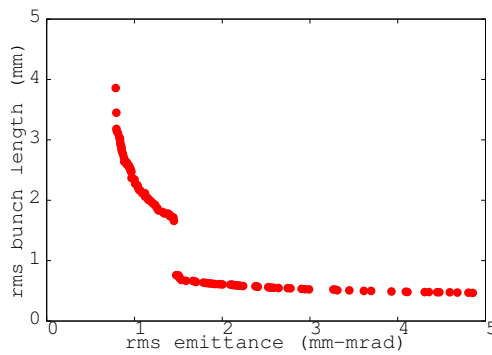


Figure 6: Optimal rms bunch length and transverse emittance solutions of the photoinjector beam dynamics optimization.

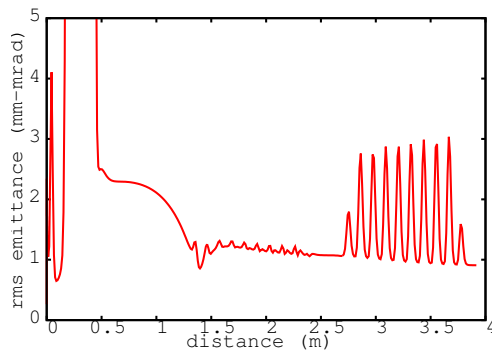


Figure 7: Transverse rms projected emittance evolution inside the photoinjector.

emittance compensation, the jump in the Pareto front, and the extension to include more RF accelerating cavities.

ACKNOWLEDGEMENT

This research used computer resources at the National Energy Research Scientific Computing Center and at the National Center for Computational Sciences.

REFERENCES

[1] I.V. Bazarov and C.K. Sinclair, *Phys. Rev. ST Accel. Beams* 8, 034202 (2005).
 [2] C. E. Papadopoulos et al., in *Proc. 35th Int. Free Electron Laser Conf.*, Malmö, Sweden, 2010, p. 479.
 [3] A. Hofler et al., *Phys. Rev. ST Accel. Beams* 16, 010101 (2013).
 [4] R. Storn and K. Price, *Journal of Global Optimization* 1a1:341-359, (1997).
 [5] K. Price, R. Storn, and J. Lampinen, *Differential Evolution - A Practical Approach to Global Optimization*, Springer, Berlin, 2005.
 [6] M. M. Ali and A. Torn, *Computers and Operations Research*, Elsevier, no. 31, p. 1703, 2004.
 [7] J. Qiang and C. Mitchell, "A Unified Differential Evolution Algorithm for Global Optimization," LBNL-6703E, 2014.
 [8] J. Qiang et al., in *Proc. 4th Int. Particle Accelerator Conf.*, Shanghai, China, 2013, p. 1031.

[9] F. Neri and V. Tirronen, *Artif. Intell. Rev.* 33, p. 61, 2010.
 [10] J. Brest et al., *IEEE Transactions on Evolutionary Computation*, vol. 10, no. 6, pp. 646-657, 2006.
 [11] J. Zhang and A. C. Sanderson, *IEEE Transactions on Evolutionary Computation*, vol. 13, no. 5, pp. 945-958, 2009.
 [12] J. Qiang et al., *Phys. Rev. ST Accel. Beams* 9, 044204 (2006).
 [13] K. Baptiste et al., *Nucl. Instrum. Methods Phys. Res., Sect. A* 599.
 [14] F. Sannibale et al., *Phys. Rev. ST Accel. Beams* 15, 103501 (2012).